CEAS Aeronautical Journal
https://doi.org/10.1007/s13272-025-00853-y

ORIGINAL PAPER

Manufacturing, modelling and testing of acoustic liners extended with flexible walls

Fleming Kohlenberg[1,2] · Moritz Neubauer[3] · Julia Genßler[1,2] · Vincent Radmann[2] · Karsten Knobloch[1]

Received: 20 December 2024 / Revised: 7 May 2025 / Accepted: 13 May 2025

Abstract
This study investigates a novel acoustic liner concept from an acoustical and manufacturing perspective. The proposed damping system combines a conventional Helmholtz resonator with additional structural resonances due to flexible walls. Promising flexible wall materials were characterised in terms of their mechanical properties by dynamic mechanical analysis and their resistance to environmental influences. Based on these results, flat liner samples with a flexible intermediate wall were designed, manufactured and experimentally tested. A process chain with a pre-tensioning device for preserving the stress state during the joining process was developed for technical production. Compared with a conventional liner, the new type of liner exhibits additional low-frequency and, in particular, broadband damping. Numerical simulations of the liner showed good agreement with the experimental results, highlighting the role of the flexible wall. In addition, broadband dissipation was observed for the same installation space compared with the reference. This type of liner was then converted into an engine-like curved structure to investigate the influence of higher acoustic modes. Therefore, the design, production, engine integration and acoustic characterisation of a new liner concept with flexible walls for low-frequency and broadband dissipation of engine noise were successfully demonstrated.

Keywords Aeroacoustics · Acoustic damping · Acoustic liner · Manufacturing · Novel liner concepts

1 Introduction

Typically, noise attenuation is most effective close to the source. Hence, an effective means of suppressing propulsion noise is the acoustic treatment of the inner walls of the nacelles, which are called acoustic liners, near the fan. A conventional acoustic liner consists of a perforated facesheet bonded to impervious honeycomb cells terminated by a rigid backing. Conventional liners are usually modelled as an array of independent Helmholtz resonators (HR). A Helmholtz resonator is a cavity with very small dimensions compared to the respective acoustic wavelength, and is connected to the exterior by a facesheet with one or multiple small holes [1]. The design parameters for such a perforated plate single-degree-of-freedom treatment panel are the perforate porosity (open area ratio) σ_{fs}, the orifice hole diameter d_{fs}, the perforate thickness h_{fs}, and the cavity depth l_{cav}. In addition, the dissipation due to the liner is affected by the mean flow Mach number Ma, the boundary layer thickness near the walls, and the incident sound intensity [2, 3].

To reduce the impact of climate change, future engines will be larger and have a slower rotation speed. This trend towards ultra-high-bypass ratio yields several challenging aspects for future acoustic liners. For example, a slower rotation frequency leads to a lower blade passing frequency and consequently to fan noise with tonal components at lower frequencies, whereas the overall noise spectrum is expected to become more broadband and less dominated by tonal content. Furthermore, the simultaneous increase in the fan diameter and decrease in nacelle length to reduce drag also reduces the effectiveness of existing acoustic liners.

✉ Fleming Kohlenberg
fleming.kohlenberg@dlr.de

1 Institute of Propulsion Technology, Engine Acoustics, German Aerospace Center (DLR), Bismarckstr. 101, 10623 Berlin, Germany

2 Institute of Fluid Dynamics and Engineering Acoustics, Technische Universität Berlin, Einsteinufer 25, 10587 Berlin, Germany

3 Institute of Lightweight Engineering and Polymer Technology (ILK), Technische Universität Dresden, Holbeinstraße 3, 01307 Dresden, Germany

Published online: 13 June 2025

In addition, the nacelle is thinned with less available liner thickness to reduce overall weight.

Therefore, future acoustic liners need to achieve higher and broader peak noise dissipation at lower frequencies than conventional liner structures with deeper cavities being not an option. Therefore, new advanced liner technologies are needed to tackle this low-frequency-broadband noise with limited installation space.

Many novel liner concepts try to enhance Helmholtz resonances by making use of new manufacturing techniques to modify the facesheet or cavity structure. This includes extending the air path in the facesheet for lower Helmholtz resonances [4–6], combining different resonators for broadband damping [7, 8] or a bent folded cavity structure with optional additional septa inserted for broadband and low-frequency damping [9–11].

To extend the Helmholtz principle, researchers have found that it is beneficial to combine Helmholtz resonators with flexible plates [12–17]. These flexible plates inhibit additional structural resonances that are tuneable independent of the Helmholtz resonance. Therefore, with well-chosen flexible materials, low-frequency noise can be damped without increasing the overall resonator volume. However, the acoustic benefit of these flexible walls was found to be higher in the vicinity of the Helmholtz resonance. Therefore, the flexible walls excel in extending the damping range near the Helmholtz resonance, rather than enabling a distinct new range.

Knobloch et al. [18] used flexible walls in a liner segment to couple cavities, proving that integrating flexible walls is beneficial for low-frequency broadband damping. Kohlenberg et al. [19] developed an analytical model to predict the impedance of a Helmholtz resonator with a small circular plate subdividing the cavity. They found good agreement with their experimental data, but their model is limited to cases in which only the first radial mode is dominant. In later works, the authors showed that in a system with larger circular plates, multiple radial modes contribute to the overall damping. With the help of a vibrometer setup or additional microphone instrumentation inside the cavity, the researchers separated Helmholtz resonances and plate-associated resonances and found stronger plate vibration when Helmholtz resonance and plate resonances were close together. The acoustical response was accurately modelled using finite element methods [20, 21].

Genßler et al. [22] experimentally investigated the position and number of flexible plates, as well as their materials, shapes and sizes. They found the plate material and, especially, its flexural rigidity to be the most sensitive parameter and concluded that a low flexural rigidity is beneficial. Neubauer et al. [23] analysed the influence of the manufacturing process and temperature on preferred flexible materials. Furthermore, Neubauer et al. [24] investigated the influence of parameters such as the Young's modulus on the flexible wall and addressed manufacturing challenges for novel acoustic liners with flexible elements. Radmann et al. [25] addressed similar challenges in the context of modelling, optimisation and usage of plate silencers as liners in turbojet engines.

This paper is structured as follows: First, the material selection process for the flexible walls is briefly discussed. This is followed by the manufacturing process, the introduction of the test facility, and the experimental and simulation results of the planar samples in Sect. 3. In addition, an annular liner sample was manufactured and tested to assess the liner performance under higher order acoustic modes. This is presented in Sect. 4. Finally, a conclusion is drawn in Sect. 5.

2 Material selection process

An analytical model of a Helmholtz resonator with a flexible wall [19] was used to determine favourable mechanical flexible wall properties. Two materials made of thermoplastics (thermopolyurethane (TPU) and ethylene butyl acrylate (EBA)) showed promising acoustical damping due to their low flexural rigidity and high mechanical loss factor. These were then selected for rigorous testing to address their applicability in aero-engines. Sample films made of TPU and EBA were characterised with regard to their mechanical properties (using dynamic mechanical analysis) and chemical resistance. The material's resistance to environmental conditions such as UV radiation, high temperatures and fluids such as water, fuel, hydraulic oil and de-icing fluid was assessed. No significant effect of water, high temperatures or de-icing fluid was found, whilst fuel reversibly increased the probe mass. However, TPU showed signs of deterioration upon exposure to hydraulic oil, and the EBA blends showed signs of embrittlement when exposed to strong UV radiation. Therefore, care has to be taken when selecting flexible wall materials for a future application inside aero-engines. TPU was then selected to be used in planar liner samples to validate the prediction models and investigate the acoustical performance with high sound pressure levels and grazing flow.

3 Planar liner

To investigate the principle of the FXW liner, several planar liner samples were investigated which are introduced in the following.

Table 1 Planar liner sample geometries

Name	h_{fs} in mm	d_{fs} in mm	σ_{fs} in %	A_{cav} in mm^2	l_{cav_1} in mm	l_{cav_2} in mm	A_{p} in mm^2	Cells
HR	1.5	1.1	6.1	19^2	42	–	–	40
FXW1	1.5	1.0	6.0	19×15.8	42	2.5	15×26	40
FXW2	1.5	1.0	6.1	19×15.5	42	2.5	15×26	36

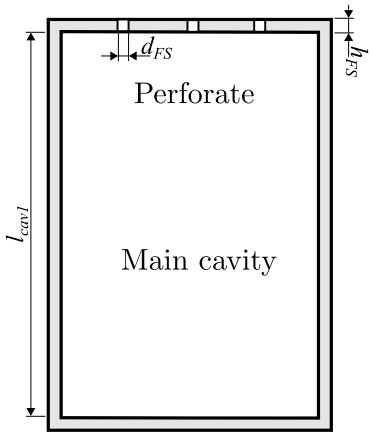

(a) Schematic cell

(b) Liner sample

Fig. 1 Schematic cell and photograph of the reference liner sample (HR)

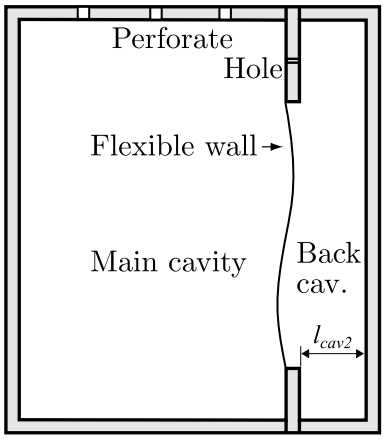

(a) Schematic cell

(b) Liner sample

Fig. 2 Schematic cell and photograph of the liner sample with one flexible wall (FXW-1)

3.1 Samples and manufacturing

Three flat liner samples were manufactured and tested: one reference sample (HR), which is a conventional single-degree-of-freedom Helmholtz resonator liner, and one flat sample with one (FXW1) and one sample with two (FXW2) flexible intermediate walls. The geometric properties of the plane liner samples are stated in Table 1, where l_{cav_2} denotes the back cavity depth and A_{p} denotes the area of the flexible plate.

A schematic cell and a photograph for each liner sample can be found in Figs. 1, 2 and 3.

For the manufacturing of flat liner samples used for comparing different cavity configurations, polyamide-6 organic sheets with 60 % continuous glass fibre reinforcement (PA6-GF) were cut to size using water jet cutting. After cutting, an adhesive film was applied to the stringers with cut-outs. Subsequently, the TPU plate material was pre-tensioned using the tensioning device described in Ref. [24] and were attached to the stringers with light pressure using the adhesive film (see Fig. 4a, b). In addition, small holes (0.6 mm) were drilled in the stringers to allow for pressure equalisation between the cavities. In the next step, the stringers were assembled and sealed with a two-component adhesive (DP490, 3 M^{TM} Scotch-Weld^{TM}) to ensure bonding and prevent the transmission of airborne sound between the cavities (see Fig. 4c). For precise positioning of the core structure, grooves were milled into the facesheet and base sheet, which were then filled with adhesive to ensure bonding between the sheets and the core structure. Figure 4d shows sample FXW2 after the completion of the assembly process. The reference liner and the FXW1 liner were manufactured by the same process.

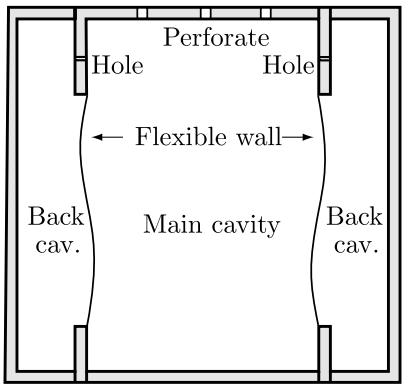

(a) Schematic cell

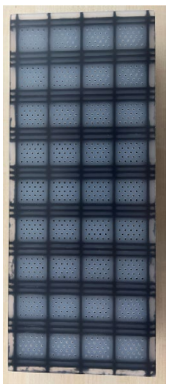

(b) Liner sample

Fig. 3 Schematic cell and photograph of the liner sample with two flexible walls (FXW-2)

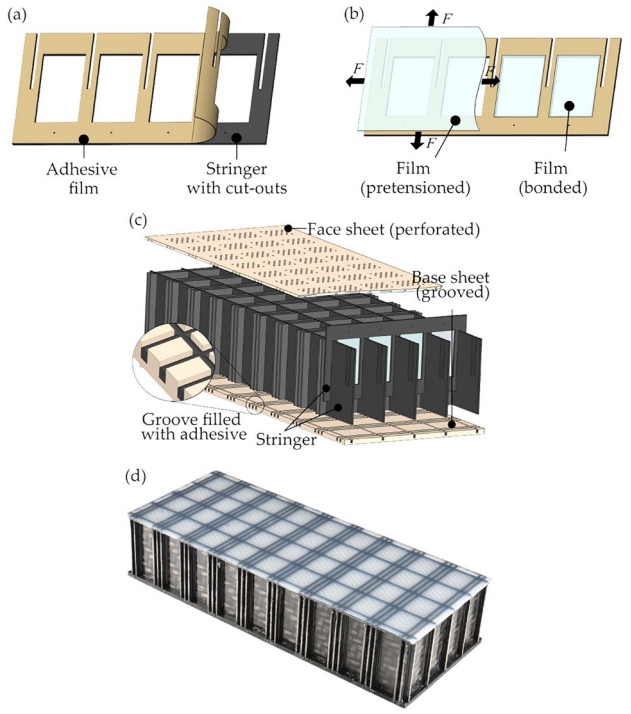

Fig. 4 Assembly process of the planar FXW liner sample: application of the adhesive film on to the stringer, **b** attaching the pre-tensioned film, **c** assembly of the planar liner, **d** finished FXW2 liner

3.2 Experimental setup: DUCT-R

The experimental investigations of the manufactured planar liner samples are conducted at the duct acoustic test rig (DUCT-R) facility of the German Aerospace Center (DLR) in Berlin. The rig is sketched in Fig. 5 and consists of two symmetrical parts with a cross-section of 60 mm × 80 mm and a cut-on frequency of the first higher mode of 2142 Hz at ambient conditions. This is the upper limit of the measurement range, as the evaluation is restricted to planar acoustic waves.

Each part is equipped with five flush-mounted microphones of type 1/4" G.R.A.S. 40 BP-S1 to decompose the sound field into upstream and downstream travelling sound waves in each section, respectively. The sound waves are excited either via upstream speaker "A" or downstream speaker "B" (see Fig. 5) of type BMS 4599HE with a single tone and an adjustable amplitude of the incoming plane wave (downstream, if excited by speaker A, upstream, if excited by speaker B) in the corresponding hard wall's section.

The decomposed sound field prior and after the test section is used to determine the energetic scattering coefficients (reflection R, transmission T, dissipation Δ) upstream and downstream of the channel with the tested resonator installed at one side of the duct. Note that the dissipation is calculated as $\Delta = 1 - R - T$, i.e. acoustic energy neither reflected nor transmitted has to be dissipated by the liner.

The test facility offers the possibility to measure the effect of grazing flow and non-linear sound excitation with sound amplitudes of more than 130 dB. The facility is well-established and has been extensively used for liner measurements and impedance eductions with a low error (< 3 %) in derived dissipation [18, 26–28].

In the context of acoustics, "attenuation", "damping" and "dissipation" are sometimes used synonymously. For improved clarity, the definitions of these terms are adapted from Morfey [29] and presented here. *Attenuation* refers to the reduction in the amplitude of an acoustic field variable, such as acoustic pressure fluctuations. *Damping* is defined as the absorption of energy in a propagating wave or the loss of energy from an oscillation system by dissipation or radiation. In this work, damping is used to describe dissipation of acoustic energy either in the air domain or the solid domain at the flexible wall. *Dissipation* is defined more general as the irreversible conversion of acoustic energy into thermal energy. In this work, dissipation is used to describe this physical mechanism as well as an abbreviation for the "dissipation coefficient".

3.3 Results

The measured dissipation of the reference sample (HR) and with one (FXW1) and two (FXW2) flexible intermediate walls with a single tone excitation at an incoming sound pressure wave of 110 dB and no grazing flow are displayed in Fig. 6. The step size is 25 Hz below 1000 Hz and 50 Hz above.

The reference sample is a simple Helmholtz resonator with one dominant damping peak around 1000 Hz (Helmholtz resonance) and a second damping peak around 1300 Hz (blue), which depends on the liner length. The FXW1 liner

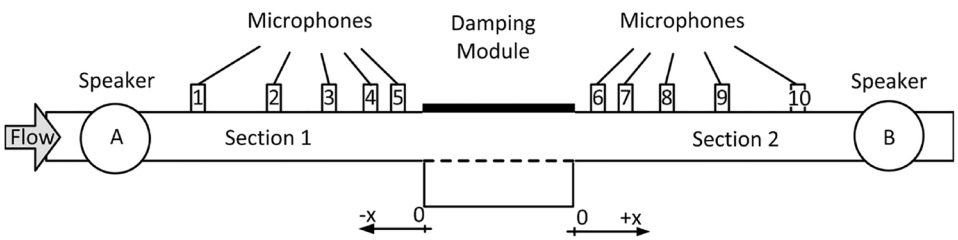

Fig. 5 Schematic view of the DUCT-R test rig

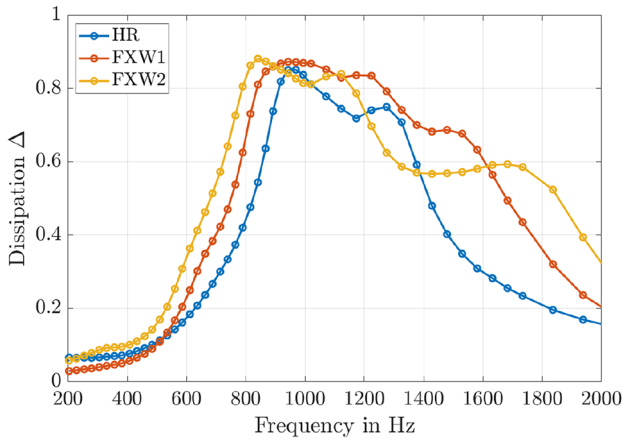

Fig. 6 Dissipation of HR liner (blue), FXW1 liner (red), and FXW2 liner (yellow), no flow

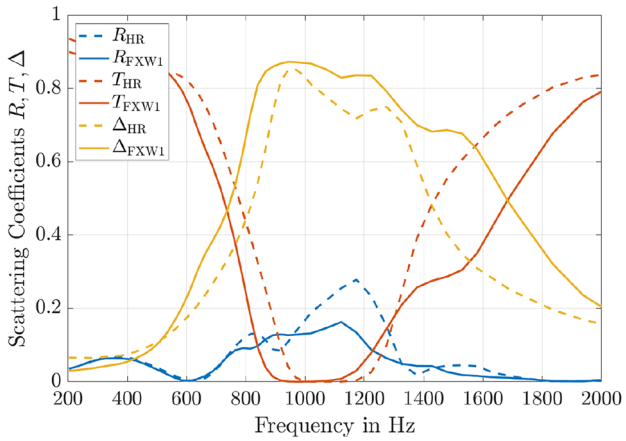

Fig. 7 Scattering coefficients of HR liner (dashed) and FXW1 liner (solid), no flow

allows for much stronger and wider damping (Δ, red) with the same available space. The FXW liners have multiple damping mechanisms: the Helmholtz resonance, which is similar to the reference sample's and additional damping due to the flexible walls. The flexible plate is made of TPU with a Young's modulus of $E = 16$ MPa, has a loss factor of $\eta = 0.1$ and a thickness of 0.3 mm. The Young's modulus and the loss factor were determined by a dynamical mechanical analysis. The same values were used in the numerical simulation. The damping is extended towards lower and higher frequencies due to multiple structural resonances[1]. Doubling the number of flexible walls in each cavity increases the acoustic effect of the flexible walls. The main dissipation peak of the FXW2 liner (yellow) is shifted towards lower frequencies even further and additional higher frequency damping is visible around 1700 Hz. However, dissipation is decreased near 1400 Hz, too.

The spectrum of all scattering coefficients for the HR and FXW1 liner is shown in Fig. 7. Note, that the measurement point marks have been dropped for better visibility.

One can see that the introduction of the flexible walls shifted the transmission (T, red) towards lower frequencies and reduced the reflection (R, blue) near the main resonance around 1100 Hz, which both contributed to an overall amplified dissipation of the novel liner concept.

The effect of a high sound pressure level and grazing flow for the reference sample is displayed in Fig. 8.

The HR liner showed higher damping at an incoming sound pressure level of 130 dB (red) compared to 110 dB (blue). This can be explained by the fact that increasing the

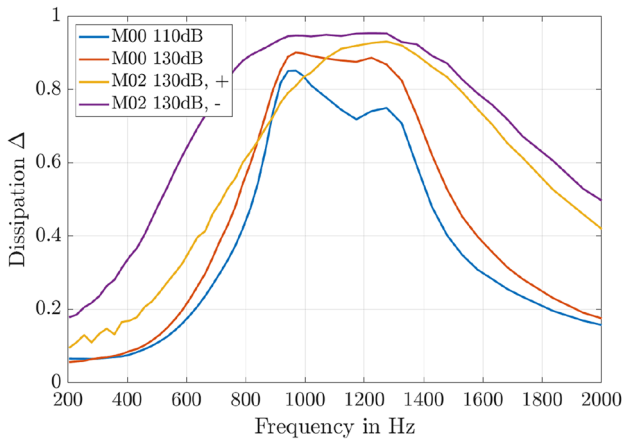

Fig. 8 Dissipation of HR liner under high sound pressure level excitation and with grazing flow

sound pressure level leads to additional losses, as acoustic energy is converted into turbulent energy due to jet formation near the Helmholtz resonance, where the sound particle velocity is at its maximum.

Introducing a grazing flow with a centre-line Mach number of Ma= 0.2 shows two things. First, the damping is increased again due to the mean flow and turbulent effects, which are beneficial for this particular liner set. Second, the damping is different in flow direction (downstream, +, yellow) and against flow direction (upstream, –, violet). This is mainly due to convective and minor due to refractive effects. Convection reduces attenuation in the flow direction because the sound waves travel faster over the silencer. Refraction is due to the boundary layer profile near the wall, which directs the sound wave towards the liner.

Similar relationships can be found for the FXW1 liner in Fig. 9.

[1] In the case of only one dominant structural resonance, the damping would be extended either towards lower *or* higher frequencies, but not both.

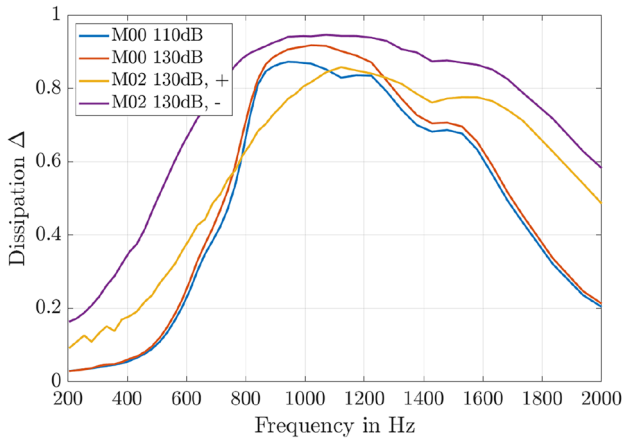

Fig. 9 Dissipation of FXW1 liner under high sound pressure level excitation and with grazing flow

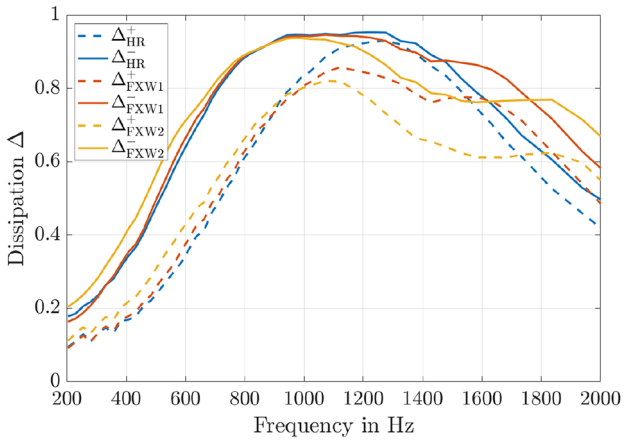

Fig. 10 Dissipation of HR liner (blue), FXW1 liner (red) and FXW2 liner (yellow) at Ma=0.2, downstream (solid) and upstream (dashed)

One can see that the higher sound pressure level mainly alters the dissipation near the Helmholtz resonance at 1000 Hz but only minor near the additional damping due to the flexible walls around 700 Hz and 1500 Hz. These results suggest that high sound pressure levels predominantly affect the acoustic properties of the facesheet but not the flexible walls in the liner samples. However, in the vicinity of the Helmholtz resonance, both the facesheet and possibly the flexible plate can behave non-linear, i.e. amplitude dependent. Therefore, a clear separation of effects is not possible. However, far away from the Helmholtz resonance, non-linear effects should only affect the flexible plate since no high sound particle velocities in the facesheet are involved. Since the dissipation changes far away from the Helmholtz resonance are smaller, we conclude that high sound pressure levels mainly affect the facesheet.

Similar to the HR liner, the dissipation of the FXW1 liner with grazing flow was higher upstream than downstream. The additional damping around 1700 Hz is visible in both directions.

Figure 10 displays a comparison between all liner samples under high sound pressure level and with grazing flow. In flow direction (dashed), the reference performs better between 1000 and 1600 Hz. This may be due to the reduced active liner area resulting from the side-mounted back cavities. The advantages of the flexible walls only appear above 1700 Hz and below 1000 Hz, but is more pronounced against the flow direction (solid). The FXW1 liner adds substantial dissipation above 1400 Hz, whilst the FXW2 liner adds low- and high-frequency dissipation. Note that neither liner has been optimised but adapted for a better comparison in the existing environment. Therefore, their geometries were chosen to allow a fair comparison between the concepts, rather than showing optimal dissipation.

3.4 Numerical simulations

The experimental characterisation was accompanied by numerical simulations using the commercial finite element software COMSOL Multiphysics® 6.1. to gain better insight into the damping mechanisms of the novel liner concept. This setup enabled us to examine key parameters such as the pressure field inside the resonator and the plate vibration, which are difficult to determine experimentally. The facesheet is modelled by an impedance boundary condition ("Interior Perforated Plate"), which is based on Ref. [30]. An additional normalised resistance of 0.1 was added to the perforated plate impedance model to account for rig specific contributions not captured in the simulation such as wall losses outside the resonator in the liner section which was determined by a reference liner. The thin flexible plate is modelled as a clamped 2D shell structure. Material losses are accounted for by the loss factor η. The acoustic losses in the cavities were accounted for by an equivalent fluid approach ("Narrow Region Acoustics"). A mesh refinement study of the model, not shown here, was conducted prior where it was revealed that ten elements per relevant length scale (smallest side length) were sufficient to resolve the plate behaviour, whilst six quadratic elements per wavelength in the air domain were sufficient to resolve the acoustic field. The simulations were restricted to the no-flow case. A cut-view of the mesh used for the FXW-1 liner finite element simulations is shown in Fig. 11.

A comparison between the simulated and experimentally determined scattering coefficients at an incoming wave amplitude of 110 dB and no flow for the reference sample is shown in Fig. 12. An excellent agreement was found for all scattering coefficients, with slight differences away from the Helmholtz resonance. Therefore, the model is able to correctly predict the liner's acoustic properties.

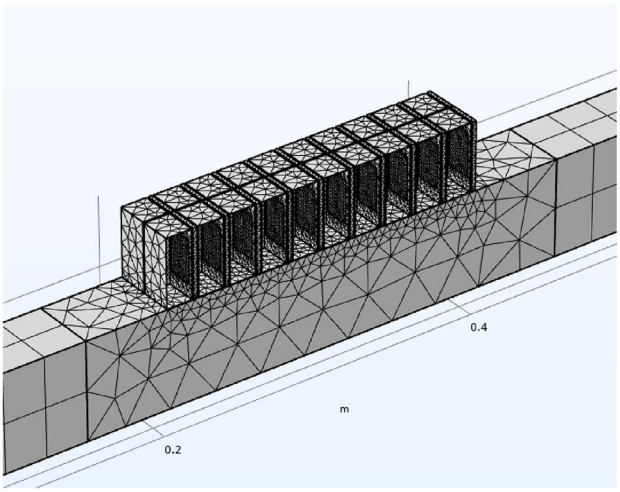

Fig. 11 Cut-view of the mesh used for the FXW-1 liner simulations

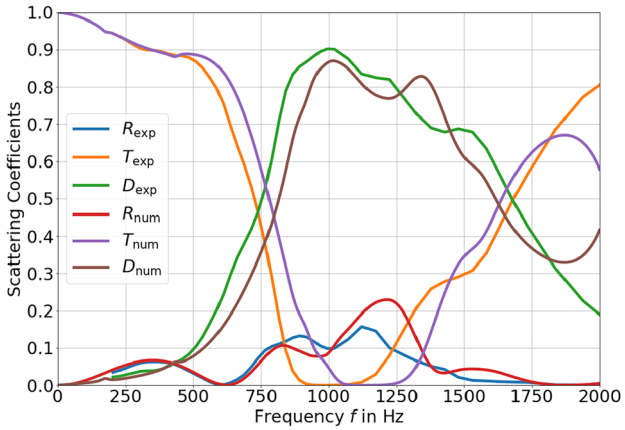

Fig. 13 Simulated and experimentally determined scattering coefficients for FXW1 liner sample at 110 dB incoming wave amplitude and no flow

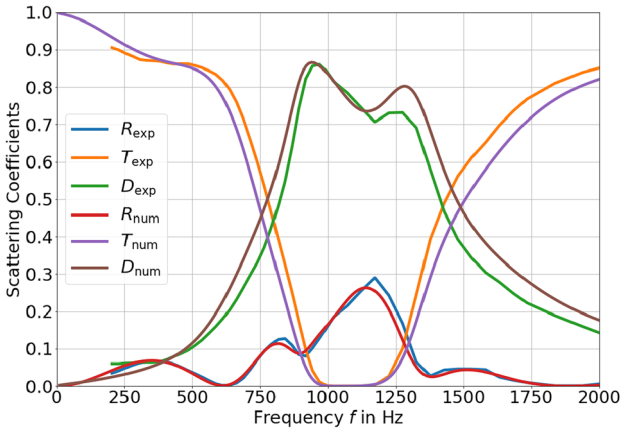

Fig. 12 Simulated and experimentally determined scattering coefficients for HR liner samples at 110 dB incoming wave amplitude and no flow

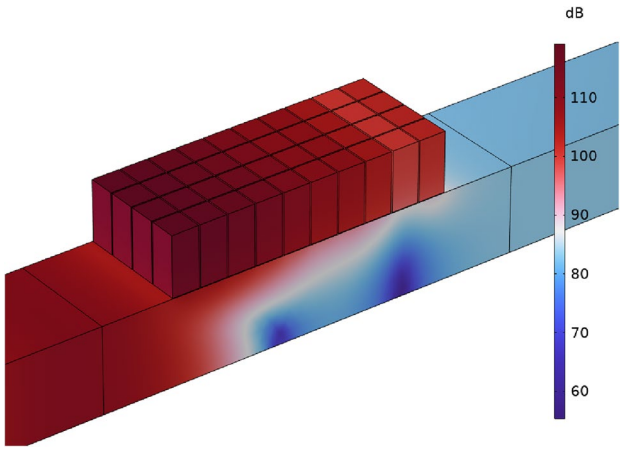

Fig. 14 Sound pressure level field for HR liner sample at 1000 Hz

The comparison between the prediction and test results of the FXW1 liner sample is depicted in Fig. 13. Again, a good agreement was found, as the numerical model correctly predicted a higher dissipation at higher frequencies (> 1000 Hz) due to the presence of the flexible walls. Some differences between the experimental and prediction results might be due to the neglection of the pre-tension of the flexible walls and the static pressure difference ("hole" in Fig. 2). In addition, the Young's modulus and loss factor of thermoplastics are temperature- and frequency-dependent, which were not considered in the numerical model. A comparison between Figs. 12 and 13 reveals that the increased dissipation around 900 Hz and 1600 Hz is mainly due to reduced transmission leaving the reflection relatively unchanged.

The validated numerical model can be used to gain a better understanding of the underlying physics of the liner concept. An exemplary simulated sound pressure field for the reference liner sample at 1000 Hz near the Helmholtz resonance frequency is depicted in Fig. 14. Note that the plane wave assumption breaks down above the liner.

The numerical simulations allow for a simultaneous analysis of the sound pressure field and the plate vibration. Both are depicted in Fig. 15 at 1000 Hz, where strong dissipation occurs. The pressure in the resonator cavities is amplified, and the plate velocity pattern shows a combination of higher order structural modes that change axially. Note that this snapshot represents a single moment in time, and the pattern changes with the incoming sound wave's phase.

Furthermore, the overall dissipation can be compared to the flexible plate's vibration, averaged over all flexible plates, which is depicted in Fig. 16.

One can see that the strongest vibrations of the flexible plates were observed near the Helmholtz resonance due to the increased pressure inside the cavities, visible in Fig. 15.

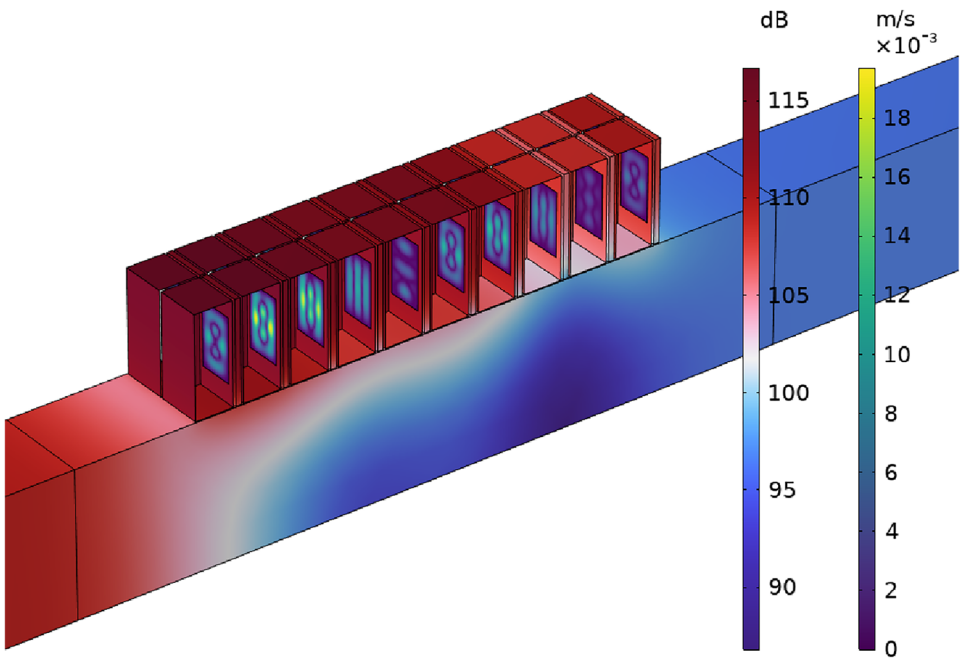

Fig. 15 Cut-view of sound pressure level field and plate velocities for FXW1 liner sample at 1000 Hz

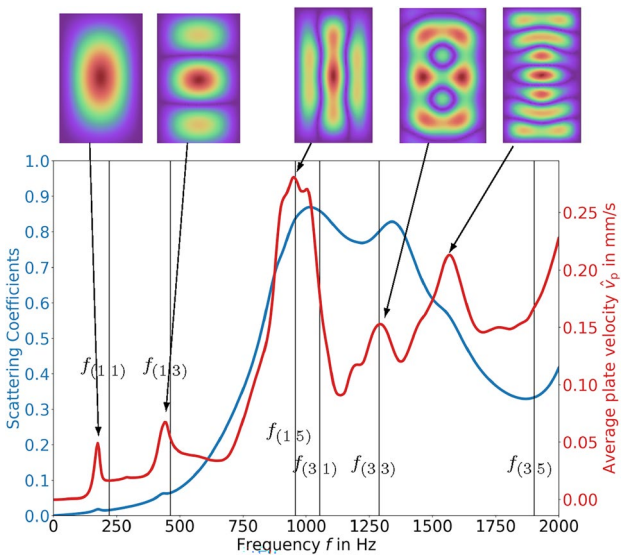

Fig. 16 Comparison between overall dissipation, average plate velocity and corresponding velocity fields of FXW1 sample

The first six uneven in-vacuo eigenfrequencies of the flexible plate are depicted with vertical lines for better comparison. The operating deflection shapes near 200 Hz and 450 Hz are close to the corresponding eigenfrequency and resemble the first and third eigenmode of the flexible wall. They show large velocities but are too far away from the Helmholtz resonance frequency to significantly contribute to the overall dissipation. Thus, one has to tune the lower eigenfrequencies of the flexible walls near the Helmholtz frequency to obtain strong additional damping. However, higher operating deflecting shapes allow for additional high-frequency damping, too. Interestingly, the velocity fields near the Helmholtz resonance do not correspond to "pure" eigenmodes, even though the in-vacuo eigenfrequency of the (1,5) mode is very close. We call these operating deflection shapes "mixed" since they are not the same as in-vacuo eigenmode shapes of a rectangular plate, found for example in Ref. [31], but appear to be a blend of different eigenmodes. This suggests that the resonance behaviour of the flexible plate is altered by the Helmholtz resonance and back cavity. Another contributing factor is that the deflection of the flexible plate depends on the pressure difference inside the cavity which is higher near the Helmholtz resonance, regardless of nearby eigenmodes. The depiction of the velocity fields in Fig. 16 is captured at the highest mean velocity; however, a closer view of Fig. 15 reveals that the shape is dependent on the phase, too.

The damping contributions of the flexible plates and the viscothermal boundaries inside the cavities are depicted in Fig. 17. The cavity losses were calculated as the difference in the total dissipation between one simulation including core losses and one simulation excluding core losses. The dissipated energy $D_{\text{plate}} = {}^{Q}/_{P_{\text{in}}}$ due to material losses is evaluated using $Q = \sigma : \text{real}(\text{i}\bar{\omega}\epsilon)$ with $:$ denoting the double-dot product and σ and ϵ denoting the stress and strain tensor of the flexible plates, respectively. P_{in} denotes the sound power of the excited incoming wave. The mechanical losses inside the flexible plate made out of TPU arise from the molecule structure, since elastomers statistically favour a coiled state in a thermodynamical equilibrium, known as entropy elasticity. When a stress is applied to an elastomer, this coiled up state is untangled which leads to high friction

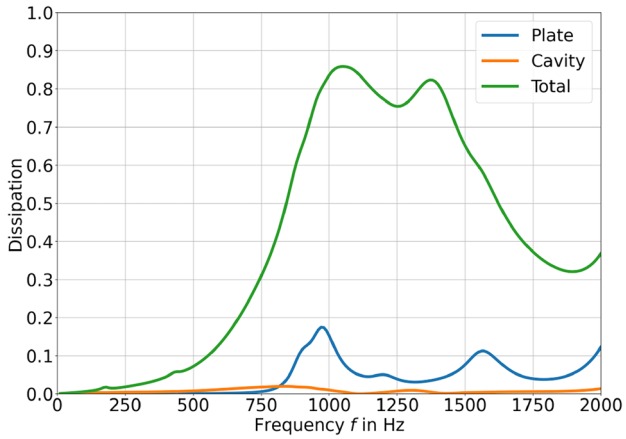

Fig. 17 Damping contributions of the flexible plates and viscothermal boundaries inside the cavities to the total FXW1 liner dissipation

between the polymer chains and subsequently to high material losses [32]. The flexible plates add substantial dissipation around 900 Hz and 1600 Hz, whilst the influence of the viscothermal boundaries at the rigid walls inside the core is negligible.

The flat liner sample investigations demonstrated the manufacturing, testing and modelling of the novel liner concept. The liner samples showed additional damping with and without grazing flow. Future optimisation is possible using the presented numerical model.

4 Annular liner

To investigate the principle of the FXW liner under realistic conditions and geometric configurations, both a annular-shaped reference demonstrator and a annular-shaped FXW demonstrator were manufactured and tested.

4.1 Samples and manufacturing

This process first involved transferring the planar geometric design of the liner sample into a three-dimensional, spatially and azimuthally symmetric annular structure. Regarding the design of the main and back in the annular-shaped FXW demonstrator, the FXW-1 configuration—with one flexible wall per main cavity—was preferred over the FXW-2 concept to simplify manufacturing. One of the most crucial points regarding the design was the determination of the appropriate width of the grooves in the top layer and in the top plate, which are required for the positioning and fastening of the core structure. Since both sheets were manufactured in a flat configuration and subsequently curved (see Fig. 18(a, b)), the resulting geometries had to be adjusted to ensure that the stringers would fit into the grooves even after forming and be properly guided. The annular liner rig was assembled in a sequential manner similar to that of the flat sample. The starting point was the assembly mould, where the facesheet was fixed between the connecting flanges for later installation in the duct. Subsequently, the cellular structure was inserted into the grooves of the facesheet by means of support ridges and adhesively joined. Following this, the partitioned top sheet was then bonded to the outer area of the core structure (see Fig. 18(c)). Radial pressure was applied via the curing mould to facilitate the curing process. Figure 18(d)) shows the completed core structure and the sequential application of the top sheet. Furthermore, the figure shows the configuration of the main and back cavity, which follows the planar FXW-1 liner design, except that the azimuthally arranged stringers are curved to match the annular geometry. In this configuration, the flexible walls are integrated into rectangular stringers that are arranged axially.

As part of the investigations, a complete annular reference liner (HR-A liner, see Fig. 19) and annular liner with flexible walls (FXW-A liner, see Fig. 20) were manufactured. The facesheet and volume of the main cavity $V_{\mathrm{cav_1}}$

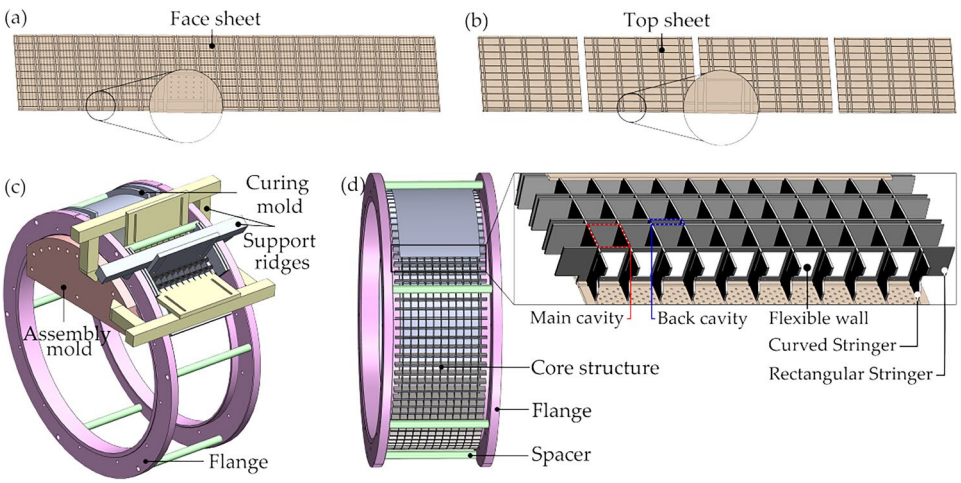

Fig. 18 Assembly process of the reference and FXW annular liner rig: **a** perforated facesheet, **b** enclosing top sheet, **c** assembly mould with core support ridges, **d** fully assembled FXW annular liner rig with detailed view of component integration

Table 2 Annular liner sample geometries

Name	h_{fs} in mm	d_{fs} in mm	σ_{fs} in %	V_{cav_1} in mm^3	V_{cav_2} in mm^3	Cells
HR-A	1.5	0.75	4.9	4710	–	1040
FXW-A	1.5	0.75	4.9	4410	750	840

was harmonised to obtain a similar Helmholtz resonance frequency of both liners for better comparison. The HR-A liner comprises a higher number of unit cells since the unit cell of the FXW-A liner also includes the volume of the back cavity V_{cav_2}. The geometric properties of both annular liners are stated in Table 2.

4.2 Experimental setup: MoSy

The manufactured annular liner samples HR-A and FXW-A were tested in the "MoSy" (Mode Synthesiser) facility. MoSy is an annular duct with an outer duct diameter of 500 mm and a centre body of 330 mm diameter, which yields a channel height of 85 mm (see Figs. 21 and 20). The facility allows the excitation and detection of specific acoustic modes. The general setup for mode synthesis and analysis was designed and applied for mode synthesis and is described extensively by Tapken [33]. The facility was recently extended to evaluate the multi-modal scattering coefficients of liners [34].

The setup is similar to that of the DUCT-R in that sense, that the liner is placed in the middle between two microphone sections, a loudspeaker section, and finally anechoic terminations. However, the larger duct geometry allows for acoustic propagation that is not restricted to plane waves in the investigated frequency range. For the MoSy, the pure plane wave propagation was limited to frequencies below 270 Hz. For higher frequencies, the sound field varies spatially over the cross-section, substantially increasing the experimental complexity.

Sound is excited with an incoming wave amplitude of 110 dB using two rings of 16 speakers (BMS 4548) each. This allows for an individual generation of circumferential mode orders $m = \{-7, \ldots, +7\}$ and radial modes of order $n = \{0, 1\}$.

The sound field is decomposed in back and forth travelling modes using two microphone arrays consisting of 98 microphones (GRAS 40BP) each with a slightly asymmetric distribution over seven rings at different axial locations. Details on the microphone array design are given in Ref. [35].

The determination of the dissipation of the liner for each mode Δ_{mn} is done via an energy balance:

$$R^{\pm}_{mn} + T^{\pm}_{mn} + \Delta^{\pm}_{mn} = 1 \tag{1}$$

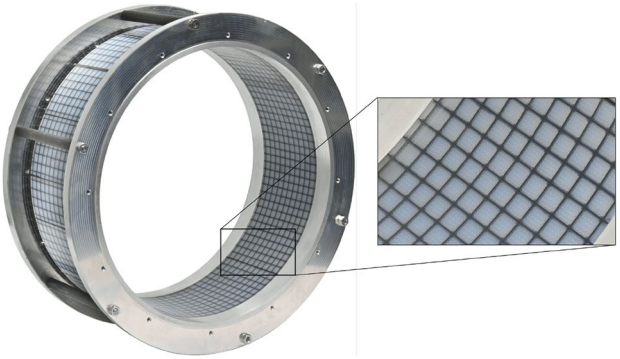

Fig. 19 Annular HR-A liner

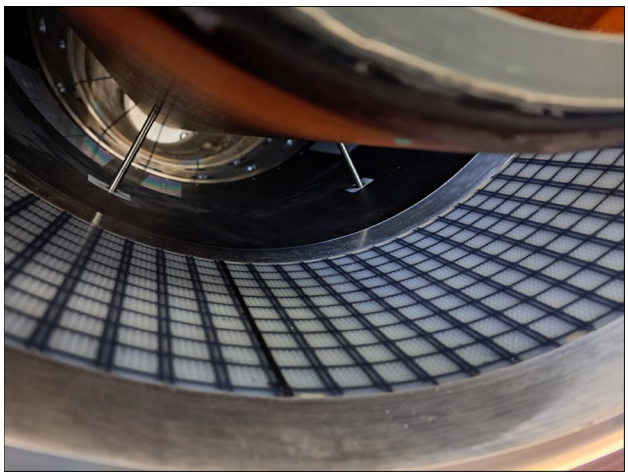

Fig. 20 Annular FXW-A liner mounted inside MoSy

with R_{mn} denoting the modal energetic reflection coefficient and T_{mn} the modal transmission coefficient. More details about determination of the scattering coefficients can be found in Ref. [34]

This mode-by-mode energy balance is only valid when mode scattering can be neglected, i.e. when no significant portion of energy of one mode is scattered into another mode due to the presence of the liner. Both annular liners are spliceless and therefore no mode scattering is expected. Mode scattering into other circumferential or radial mode orders can be assessed by the full evaluation of the microphone arrays on both sides of the liner barrel. The difference between the excited mode and the second strongest mode found on the reflection side (close to the excitation) and the

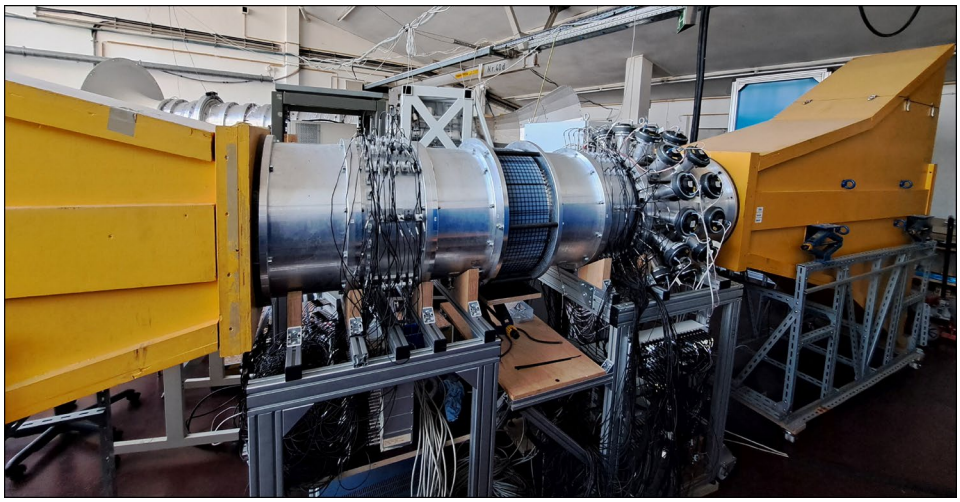

Fig. 21 MOSY setup for annular duct measurements including speaker array, two microphone sections and the liner test section in between

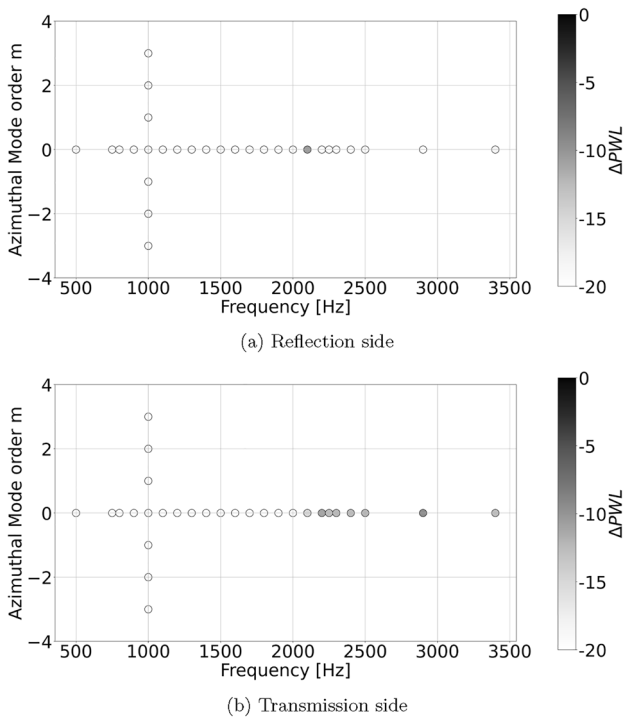

Fig. 22 Sound power level difference between excited mode and second strongest mode

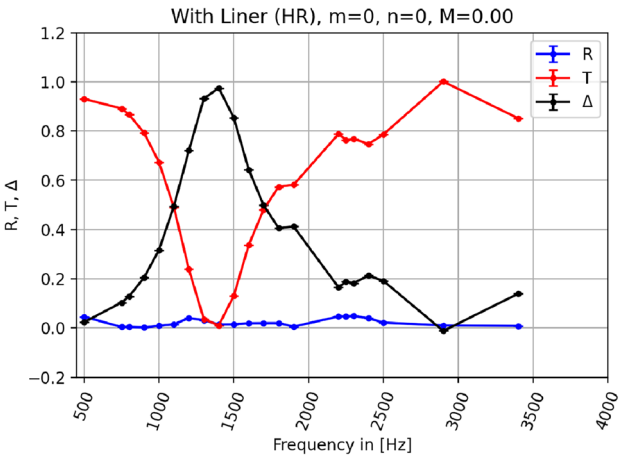

Fig. 23 Scattering coefficients of HR-A liner (plane wave)

transmission side, i.e. after the attenuation of the sound field by the liner barrel, is presented in Fig. 22.

For the vast majority of the measured cases, the sound power level of the excited mode is at least 10 dB higher than the second strongest mode—often even more than 20 dB. Figure 22a shows that individual modes can be excited with a large signal-to-noise ratio, as all other modes are sufficiently suppressed. Figure 22b shows that the targeted mode remains dominant after transmission over the lined section. This justifies the assumption to calculate the scattering coefficients and especially the dissipation on a mode-by mode basis. The difference drops above 2000 Hz since several modes become cut-on, e.g. (0,1) at 2035 Hz, (1,1) at 2054 Hz, (8,0) at 2066 Hz, (2,1) at 2109 Hz, and (3,1) at 2200 Hz. This "density of modes" with small propagation angles makes it more difficult to excite and distinguish between individual modes in the mode decomposition.

4.3 Measurement results

The scattering coefficients of the reference annular sample of the plane wave (HR-A) are displayed in Fig. 23. The Helmholtz resonance dominates the dissipation spectrum at 1400 Hz, with little reflection of acoustic energy. This dissipation is higher than that of the plane liner sample, mainly because of the smaller hole diameter in the facesheet.

Figure 24 displays the reflection R, transmission T and dissipation Δ of the liner with flexible walls (FXW-A).

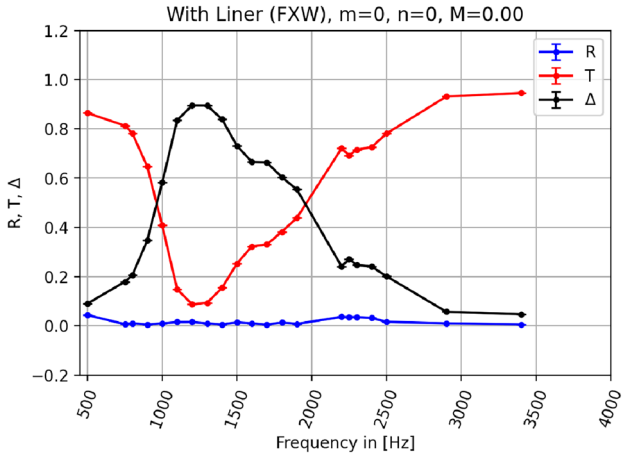

Fig. 24 Scattering coefficients of FXW-A liner (plane wave)

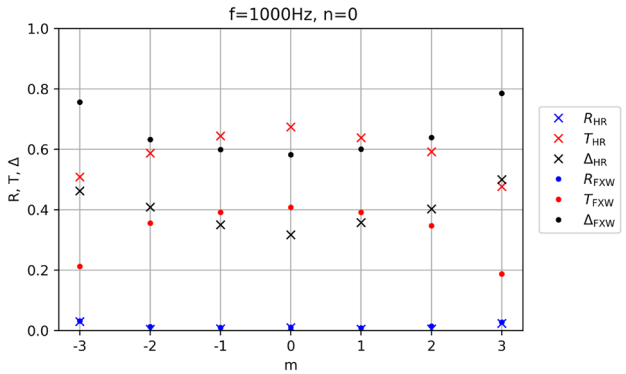

Fig. 25 Scattering coefficients of higher order acoustic modes of HR-A and FXW-A liner (1000 Hz)

One can see that the dissipation spectrum has shifted towards lower frequencies and has become much more broadband with additional damping especially between 1500 and 2000 Hz. However, the peak dissipation has decreased as well.

In Fig. 25, the scattering coefficients for multiple azimuthal modes at 1000 Hz are presented. The FXW-A liner exhibits higher low-frequency dissipation than the HR-A liner. In addition, the plane wave is the least attenuated mode with the highest uncertainty. This can be explained with the mode angle concept. Higher azimuthal modes have a sharper mode angle (near cut-off close to 90 °) than the plane wave. Therefore, they are reflected more often in their propagation path in the lined section which leads to higher dissipation. The symmetry of both liners shows that the dissipation of the higher order azimuthal modes of both annular liners is independent of the spinning direction.

5 Conclusion

The results of this study demonstrate significant progress in the understanding, modelling and manufacturing of acoustic liners with flexible walls. Promising flexible materials were tested for static and dynamic loads and chemical resistance. Good suitability was found for TPU materials. The manufacturing capabilities were successfully advanced to fabricate flat liner prototypes with and without flexible walls made of TPU and transfer the concept to curved structures. These prototypes were then acoustically characterised in the DUCT-R and MoSy test facilities. The liner structures showed excellent acoustic performance, which was better than that of the conventional samples. One additional flexible wall extends the dissipation spectrum by additional structural resonances, which was confirmed by the accompanying numerical simulations. The usage of two flexible walls leads to a stronger effect but increases manufacturing complexity. Grazing flow mainly alters the perforate acoustic properties, given that a static pressure release between the main cavity and back cavity is implemented. The annular liner tests showed that the liner concept is also beneficial in a more realistic engine-like setting. Thus, the concept of a Helmholtz resonator liner with flexible walls was proved to be suitable both conceptually and practically. The process analyses presented herein provide an essential basis for future applications of the liner concept to effectively reduce aircraft noise.

Acknowledgements This work was mainly funded within the framework of the LuFo VI-1 project "FLIER" (Flexible wall structures for acoustic Liners, contract number 20E1915B) by the Federal Ministry for Economic Affairs and Climate Action based on a decision of the German Bundestag, which is gratefully acknowledged. Further support of MoSy measurements was obtained for LuFo project MUTE (20T1915D). The authors want to thank the DLR workshop team and further colleagues of the DLR Department of Engine Acoustics for their support in the setup, measurement and data processing of the liner barrel. The fruitful collaboration within the consortium (TU Berlin, TU Dresden, BTU Cottbus-Senftenberg) and the external participants Fraunhofer IAP Schwarzheide, Fraunhofer PYCO Wildau, RRD and DLR have made the project's success possible.

Author contributions F.K. designed and conducted the acoustic experiments and numerical simulations and prepared the manuscript. M.N. designed and manufactured the samples. J.G. designed and conducted the acoustic experiments. V.R. helped in the design and conduction of the numerical simulations. K.K. designed and conducted the acoustic experiments and supervised the work. All authors discussed the results and commented on the manuscript at all stages.

Funding Open Access funding enabled and organized by Projekt DEAL. Openaccess funding enabled and organized by Projekt DEAL.

Data availability Datasets generated during the current study are available from the corresponding author on reasonable request.

Declarations

Conflict of interest The authors have no conflict of interest to declare that are relevant to the content of this article.

References

1. Strutt Rayleigh, J.W.: V. on the theory of resonance. Philos. Trans. R. Soc. Lond. **161**, 77–118 (1871). https://doi.org/10.1098/rstl.1871.0006
2. Jones, M., Tracy, M., Watson, W., Parrott, T.: Effects of liner geometry on acoustic impedance. In: 8th AIAA/CEAS Aeroacoustics Conference & Exhibit, Breckenridge, Colorado (2002). https://doi.org/10.2514/6.2002-2446
3. Motsinger, R.E., Kraft, R.E.: Design and performance of duct acoustic treatment. Technical Report NASA Reference Publication 1258, vol. 2 WRDC Technical Report 90-3052, National Aeronautics and Space Administration
4. Simon, F.: Long elastic open neck acoustic resonator for low frequency absorption. J. Sound Vib. **421**, 1–16 (2018). https://doi.org/10.1016/j.jsv.2018.01.044
5. Yang, C., Zhang, P., Jacob, S., Trigell, E., Åbom, M.: Investigation of extended-tube liners for control of low-frequency duct noise. AIAA J. **59**(10), 4179–4194 (2021). https://doi.org/10.2514/1.J059988
6. Kreitzman, J.R.: Conceptual design and validation of a bent-perforation-path acoustic liner. Technical Report NASA/TM–20230018517, National Aeronautics and Space Administration(2024)
7. Jones, M., Howerton, B., Ayle, E.: Evaluation of parallel-element, variable-impedance, broadband acoustic liner concepts. In: 18th AIAA/CEAS Aeroacoustics Conference (33rd AIAA Aeroacoustics Conference), Colorado Springs, Colorado (2012). https://doi.org/10.2514/6.2012-2194
8. Brown, M.C., Jones, M.G.: Evaluation of variable facesheet liner configurations for broadband noise reduction. In: AIAA AVIATION 2020 FORUM, Reno, Nevada (2020). https://doi.org/10.2514/6.2020-2616
9. Palani, S., Murray, P., McAlpine, A., Sasaki, D., Richter, C.: Slanted septum and multiple folded cavity liners for broadband sound absorption. Int. J. Aeroacoust. **20**(5–7), 633–661 (2021). https://doi.org/10.1177/1475472X211023835
10. Ross, E.P., Figueroa-Ibrahim, K.M., Morris, S.C., Sutliff, D.L., Bennett, G.J.: Evaluating an additive manufactured acoustic metamaterial using the advanced noise control fan. AIAA J. (2024). https://doi.org/10.2514/1.J063384
11. Sun, Y., Liu, C., Song, X., Xu, X., Zhou, J., Ma, F.: An ultrathin high-order micro-perforated meta-liner for broadband sound attenuation under grazing flow. Int. J. Mech. Sci. **294**, 110228 (2025). https://doi.org/10.1016/j.ijmecsci.2025.110228
12. Horowitz, S.B., Nishida, T., Cattafesta, L.N., Sheplak, M.: Characterization of a compliant-backplate Helmholtz resonator for an electromechanical acoustic liner. Int. J. Aeroacoust. **1**(2), 183–205 (2002). https://doi.org/10.1260/147547202760236969
13. Liu, F., Horowitz, S., Nishida, T., Cattafesta, L., Sheplak, M.: A multiple degree of freedom electromechanical Helmholtz resonator. J. Acoust. Soc. Am. **122**(1), 291–301 (2007). https://doi.org/10.1121/1.2735116
14. Nudehi, S.S., Duncan, G.S., Farooq, U.: Modeling and experimental investigation of a Helmholtz resonator with a flexible plate. J. Vib. Acoust. (2013). https://doi.org/10.1115/1.4023810
15. Sanada, A., Tanaka, N.: Extension of the frequency range of resonant sound absorbers using two-degree-of-freedom Helmholtz-based resonators with a flexible panel. Appl. Acoust. **74**(4), 509–516 (2013). https://doi.org/10.1016/j.apacoust.2012.09.012
16. Solano, C., Cattafesta, L.: Modeling, design, and optimization of a dielectric elastomer acoustic liner. Int. J. Aeroacoust. **22**(5–6), 599–620 (2023). https://doi.org/10.1177/1475472X231199187
17. Hossain, M.R., Ross, E.P., Bennett, G.J.: Acoustic plate-valve resonator for low-frequency sound absorption. AIP Adv. (2023). https://doi.org/10.1063/5.0142908
18. Knobloch, K., Enghardt, L., Bake, F.: Investigation of flexible walls for acoustic liners. In: 25th AIAA/CEAS Aeroacoustics Conference, Delft, The Netherlands (2019). https://doi.org/10.2514/6.2019-2565
19. Kohlenberg, F., Schulz, A., Enghardt, L., Knobloch, K.: Modeling of advanced Helmholtz resonator liners with a flexible wall. AIAA J. **61**(7), 3108–3118 (2023). https://doi.org/10.2514/1.J062227
20. Kohlenberg, F., Radmann, V., Genßler, J., Enghardt, L., Knobloch, K.: Experimental and numerical analysis of the vibro-acoustic behavior of a Helmholtz resonator with a flexible wall. In: AIAA AVIATION 2023 Forum, San Diego, California (2023). https://doi.org/10.2514/6.2023-3348
21. Kohlenberg, F., Knobloch, K.: Experimental and numerical parameter study of a Helmholtz resonator with a flexible wall. In: 30th AIAA/CEAS Aeroacoustics Conference (2024). American Institute of Aeronautics and Astronautics, Rome, Italy (2024). https://doi.org/10.2514/6.2024-3077
22. Genßler, J., Kohlenberg, F., Knobloch, K., Enghardt, L.: Experimental investigations of flexible wall effects in Helmholtz resonators for aircraft engine acoustic liners. In: AIAA AVIATION 2023 Forum, San Diego, California (2023). https://doi.org/10.2514/6.2023-3347
23. Neubauer, M., Pohl, M., Kucher, M., Böhm, R., Höschler, K., Modler, N.: DMA of TPU films and the modelling of their viscoelastic properties for noise reduction in jet engines. Polymers (2022). https://doi.org/10.3390/polym14235285
24. Neubauer, M., Genßler, J., Radmann, V., Kohlenberg, F., Pohl, M., Böhme, K., Knobloch, K., Sarradj, E., Höschler, K., Modler, N., Enghardt, L.: Experimental and numerical investigation of novel acoustic liners and their design for aero-engine applications. Aerospace **10**(1), 5 (2023). https://doi.org/10.3390/aerospace10010005
25. Radmann, V., Kohlenberg, F., Sarradj, E.: Modeling of a 3D plate resonator liner and comparison to numerical and experimental investigations. In: AIAA AVIATION 2023 Forum, San Diego, California (2023). https://doi.org/10.2514/6.2023-3639
26. Lahiri, C., Enghardt, L., Bake, F., Sadig, S., Gerendás, M.: Establishment of a high quality database for the acoustic modeling of perforated liners. J. Eng. Gas Turbines Power (2011). https://doi.org/10.1115/1.4002891
27. Busse-Gerstengarbe, S., Bake, F., Enghardt, L., Jones, M.G.: Comparative study of impedance eduction methods, part 1: DLR tests and methodology. In: AIAA-2013-2124. 19th AIAA/CEAS Aeroacoustics Conference, Berlin, Germany (2013). https://doi.org/10.2514/6.2013-2124

28. Schulz, A.: Die akustischen randbedingungen perforierter wandauskleidungen in strömungskanälen: Physikalische modelle und eduktion. PhD thesis, Technische Universität Berlin, Berlin (2019). https://doi.org/10.14279/depositonce-7943
29. Morfey, C.L.: Dictionary of Acoustics. Academic Press, San Diego (2001)
30. Crandall, I.B.: Theory of Vibrating Systems and Sound. D. Van Nostrand Company, New York (1926)
31. Wang, C.Y.: Structural Vibration: Exact Solutions for Strings, Membranes, Beams, and Plates. CRC Press, Hoboken (2014)
32. Popov, V.L.: Contact Mechanics and Friction. Springer, Berlin (2017). https://doi.org/10.1007/978-3-662-53081-8
33. Tapken, U.: Analyse und synthese akustischer interaktionsmoden von turbomaschinen. Dissertation, Technische Universität Berlin, Berlin, Deutschland (2016). https://doi.org/10.14279/depositonce-5124
34. Knobloch, K., Grizewski, L., Kohlenberg, F., Behn, M., Genssler, J.: Framework for modal based assessment of liner structures. In: 30th AIAA/CEAS Aeroacoustics Conference. American Institute of Aeronautics and Astronautics, Rome, Italy (2024). https://doi.org/10.2514/6.2024-3298
35. Behn, M., Klähn, L., Tapken, U.: Comprehensive experimental investigation of mode transmission through stator vane rows: results and calibration of an analytical prediction model. In: 23rd AIAA/CEAS Aeroacoustics Conference, Denver, Colorado (USA) (2017). https://doi.org/10.2514/6.2017-3218